STAAARTE-MED 1998 summer airborne measurements over the Aegean Sea
2. Aerosol scattering and absorption, and radiative calculations

Paola Formenti,[1,6] Olivier Boucher,[1,2] Thomas Reiner,[1] Detlev Sprung,[1] Meinrat O. Andreae,[1] Manfred Wendisch,[3] Heike Wex,[3] Dave Kindred,[4] Maria Tzortziou,[5] Alexandros Vasaras,[5] and Christos Zerefos[5]

Received 23 November 2001; revised 19 April 2002; accepted 24 April 2002; published 5 November 2002.

[1] Chemical, physical, and optical measurements of aerosol particle properties within an aged biomass-burning plume were performed on board a research aircraft during a profile descent over a ground-based site in northeastern Greece (40°24′N, 23°57′E; 170 m asl) where continuous measurements of the spectral downwelling solar irradiance (global, direct, and diffuse) are being made. The aerosol optical depth measured at the ground during the time of overflight was significantly enhanced (0.39 at a wavelength of 500 nm) due to a haze layer between 1 and 3.5 km altitude. The dry particle scattering coefficient within the layer was around 80 Mm^{-1}, and the particle absorption coefficient was around 15 Mm^{-1}, giving a single scattering albedo of 0.89 at 500 nm (dry state). The black carbon fraction is estimated to account for 6–9% of the total accumulation mode particle mass (<1 μm diameter). The increase of the particle scattering coefficient with increasing relative humidity at 500 nm is of the order of 40% for a change in relative humidity from 30 to 80%. The dry, altitude-dependent, particle number size distribution is used as input parameter for radiative transfer calculations of the spectral short-wave, downwelling irradiance at the surface. The agreement between the calculated irradiances and the experimental results from the ground-based radiometer is within 10%, both for the direct and the diffuse components (at 415, 501, and 615 nm). Calculations of the net radiative forcing at the surface and at the top of the atmosphere (TOA) show that due to particle absorption the effect of aerosols is much stronger at the surface than at the TOA. Over sea the net short-wave radiative forcing (daytime average) between 280 nm and 4 μm is up to −64 W m^{-2} at the surface and up to −22 W m^{-2} at the TOA. *INDEX TERMS:* 0305 Atmospheric Composition and Structure: Aerosols and particles (0345, 4801); 0365 Atmospheric Composition and Structure: Troposphere—composition and chemistry; 9335 Information Related to Geographic Region: Europe; *KEYWORDS:* aerosols, Aegean Sea, optical properties, vertical profiles, direct radiative forcing

Citation: Formenti, P., et al., STAAARTE-MED 1998 summer airborne measurements over the Aegean Sea, 2, Aerosol scattering and absorption, and radiative calculations, *J. Geophys. Res.*, *107*(D21), 4451, doi:10.1029/2001JD001536, 2002.

1. Introduction

[2] The determination of aerosol properties relevant to their effect on the Earth's radiative budget is affected by several uncertainties due both to the limitations of the sampling and measurement devices and to the difficulties in modeling the aerosols, as well as their interaction with the solar radiation. As a result, the level of scientific understanding of the climate forcing by aerosols is classified as "low" to "very low" by the *Intergovernmental Panel on Climate Change* (*IPCC*) [2001], depending on the aerosol type and the forcing mechanism considered.

[3] To overcome these difficulties, and also to check for the consistency of collected data with the working hypothesis of the models, the concept of "closure" is adopted. The term "closure" describes an attempt to measure/calculate one specific property or to test one particular assumption using an overdetermined (redundant) set of quantities or various independent methods [*Ansmann et al.*, 2002]. One typical example of a closure study is the comparison of measured and calculated particle scattering coefficient. The measured particle scattering coefficient is obtained e.g. from nephelometer data, the calculated one is derived with independent Mie calculations on the basis of the measured particle size distribution and the particle chemical composition. This comparison can be used to test

[1]Max Planck Institute for Chemistry, Mainz, Germany.
[2]On sabbatical from Laboratoire d'Optique Atmosphérique, Lille, France.
[3]Institute for Tropospheric Research, Leipzig, Germany.
[4]Meteorological Research Flight, Met Office, Farnborough, UK.
[5]Laboratory of Atmospheric Physics, Aristotle University, Thessaloniki, Greece.
[6]Now at Centre of Geophysics of Évora, Évora, Portugal.

0148-0227/02/2001JD001536$09.00

the appropriateness of the scattering theory, or the degree of mixing of the various chemical constituents.

[4] In this paper we present a case study for a closure experiment chosen from three measurement flights onboard the UK Met Office Hercules C-130 aircraft that were performed during August 1998 in the eastern Mediterranean between Thessaloniki and Crete. The original aim of these flights, part of the Scientific Training and Access to Aircraft for Atmospheric Research Throughout Europe (STAAARTE-MED) project, was the investigation of the enhanced concentrations of SO_2 and aerosol particles (mainly sulfates) that are typically found in this area mainly during the summer [*Eisinger and Burrows*, 1998; *Zerefos et al.*, 2000]. The data from the STAAARTE-MED campaign have further been analyzed by *Formenti et al.* [2002], who showed how a large biomass-burning plume was detected in the Thessaloniki area. This plume, extending with nearly constant properties over 200 km, was characterized on 14 August 1998 during a profile descent over a ground-based site located at the Mount Athos Observatory (MAO, 40°24′N, 23°57′E; 170 m asl), where concurrent measurements of the spectral downwelling solar irradiances (global, direct, and diffuse components) are being performed. The plume had aged at least six days since emission, and probably originated from fires in Canada.

[5] In this paper we discuss the aerosol particle measurements made during this profile descent, and the implications for the direct climate forcing by aerosols. First we look at the local closure of the airborne measurements of the dry aerosol particle scattering and absorption coefficients with the dry particle size distribution, which has been measured onboard together with the aerosol particle chemical composition. Similar tests have been performed by several authors [*Schmid et al.*, 2000; *Kato et al.*, 2000; *Wex et al.*, 2002]. Typically, agreement between measured and calculated aerosol particle scattering coefficients in these studies was within 20%, as long as the aerosol particle distribution did not contain significant amounts of dust. In the second part of the paper we look at the agreement between the spectral vertically integrated particle extinction coefficient (sum of the absorption and the scattering coefficients) and the particle optical depth derived from the direct solar irradiance measured at the ground-based station. This type of comparison has been discussed, amongst others, by *Kato et al.* [2000]. Finally, we compare the measured spectral downwelling irradiances with the results of radiative transfer calculations using the airborne particle size distribution as input parameter. This aspect is of interest as previous investigations have shown that often the modeled diffuse component exceeds the measurement, suggesting the existence of an unknown atmospheric absorber [*Halthore*, 1999]. A literature review of previous results on this subject is reported by *Wendisch et al.* [2002].

2. Instrumentation

2.1. Airborne Data

[6] The instrumentation was operated on board the Hercules C-130 aircraft of the United Kingdom Meteorological Office (UKMO). The aircraft has a maximum endurance of 12 h (with fuel tank reserves). Depending on flight safety regulations the minimum flight altitude is 17 m over water and 35 m over land. Maximum flight altitude is ~11000 m.

2.1.1. Aerosol Particle Size Distributions

[7] Aerosol particle size distributions are measured on board the C-130 with a Passive Cavity Aerosol Spectrometer Probe (PCASP-100X, PMS Inc., Boulder, Colorado). The PCASP is a single particle counter. Its measurement principle is based on light scattering by individual particles, which is a function of their size. In this way the PCASP classifies particles into 15 size channels in the diameter range between 0.1 and 3 μm (nominal). However, light scattering also depends on the refractive index and the humidity state of the particles. Because the PCASP is calibrated in the laboratory using latex spheres (complex refractive index equal to of $1.58 - 0i$), the particle sizing needs to be adjusted based on the actual aerosol composition estimated from filter sampling. The correction is based upon Mie calculations of the response functions of the instrument to changes in the refractive index. As shown by *Collins et al.* [2000], the size bin threshold settings are particularly sensitive to the imaginary part of the refractive index, and neglecting absorption causes particles (particularly supermicron) to be undersized. Humidity affects the size of the particles and so any drying of the sample within the PCASP will make the particles smaller than in their ambient atmospheric state. There is inherent heating within the PCASP, which was enhanced here because the PCASP was operated with de-icing heaters in front of the unit. Therefore the PCASP particle size distributions are considered dehydrated. Particle shape also influences light scattering, but the effect of nonsphericity almost cancels out in the angular collection range of the PCASP (35°–120°) [*Collins et al.*, 2000] and therefore it is neglected.

2.1.2. Aerosol Particle Scattering and Backscattering Coefficients

[8] The particle scattering σ_s and backscattering σ_{bs} coefficients (in Mm^{-1}, equivalent to 10^{-6} m^{-1}) are measured at 450, 550, and 700 nm using a three-wavelength integrating nephelometer (TSI 3563, TSI Inc., St. Paul, Minnesota). Air is sampled at 100 L min^{-1} through a semi-isokinetic inlet with cutoff at approximately 1-μm diameter. The sample relative humidity (RH_0) is maintained below 50% by heating. The instrument is calibrated in the laboratory using particle-free air (zero) and CO_2 (span gas). Zero-air checks are repeated several times during flight.

[9] A measurement uncertainty analysis is done according to *Anderson and Ogren* [1998]. Uncertainties due to calibration, drift, and noise are estimated to be within 10%. Deviations from the ideal angular response of the nephelometer are an additional source of error. These are due to noncosine weighted angular light intensity distribution of the illumination light provided by the opal glass diffuser, and to truncation of the scattered radiation at scattering angles smaller than 7° and larger than 170°. *Anderson and Ogren* [1998] have provided empirical relationships to estimate the total correction factors C_t, which have been applied to our measurements. Correction factors C_g due to near-forward and backward truncation alone can be estimated by calculating the total scattering and backscattering coefficients in the scattering angular range 7°–170° and

90°–170° (as actually measured by the nephelometer) from the particle size distributions measured by PCASP, which sampled from its own air inlet. The difference between C_t and C_g represents the effect of the quasi-Lambertian diffuser. Agreement between measured and calculated scattering and backscattering coefficients is suggestive of representative particle sampling by both systems and negligible particle losses.

2.1.3. Aerosol Particle Absorption Coefficients

[10] A Particle Soot Absorption Photometer (PSAP, Radiance Research, Seattle, Washington) measured the aerosol particle absorption coefficient σ_a at 567 nm. This instrument continuously collects particles on a glass-fiber filter (at a flow rate of 3 L min^{-1} through a semi-isokinetic inlet, cutoff at 1-μm diameter) that is illuminated by a light source (spectrally filtered light). From the temporal change of the transmission of the loaded filter the absorption coefficient of the particles deposited on the filter is derived. Errors in the PSAP measurement can arise from (1) unit-to-unit variability of the instruments; (2) instrumental noise; (3) inaccurate knowledge of operational parameters (filter spot size and air flow rate); (4) scattering particles being misinterpreted as absorption; (5) overestimate of absorption from multiple scattering. *Bond et al.* [1999] have discussed these uncertainties. The largest error (around 22%) is due to the misinterpretation of multiple scattering as absorption. The analytical formula provided by *Bond et al.* [1999] for correcting the raw PSAP data for the errors (1)–(5) were applied to the STAAARTE-MED PSAP data.

2.1.4. Water-Soluble Aerosol Particles

[11] The aerosol sampling system, using an isokinetic inlet, has been described in *Andreae et al.* [2000]. Aerosols are sampled with two sequential 90-mm diameter filters on polyethylene supports. The first stage consists of a Nuclepore filter (nominal pore size 8.0 μm), the second of a PTFE Teflon filter (nominal pore size 1.0 μm). The 50% cutoff diameter of the 8 μm Nuclepore filter is about 1.4 μm for particles with a density of 1.33 g cm^{-3} at a face velocity of about 40 cm s^{-1} [*John et al.*, 1983]. Samples are collected only during horizontal flight legs lasting not less than 20–30 min in order to guarantee sufficient loading of the filter samples. Immediately after each flight, the loaded filters are stored in 30 mL HDPE bottles, and kept in a refrigerator until extraction.

[12] Samples are analyzed for majors anions (SO_4^{2-}, Cl^-, NO_3^-) and cations (Na^+, NH_4^+, K^+, Mg^{2+}, Ca^{2+}) using Ion Chromatography (IC). Anions are determined using a Shimadzu HIC-6A ion chromatograph with a DIONEX Ion Pac AS11, 4 mm column and a conductivity suppressor (Dionex ASRS-1) before conductivity detection. The flow rate of the eluent (NaOH in gradient mode) is 1 mL min^{-1}. For the cation analysis we used a Shimadzu Ion Pac CS14, 4 mm column. The flow rate of the eluent (10 mM methanesulfonate in isocratic mode) is 1.2 mL min^{-1}. In the following discussion, concentrations are expressed as molar mixing ratios in air (ppt = pmol mol^{-1}) or as mass concentrations (μg m^{-3}) at standard temperature and pressure. The accuracy of the calibration with mono-ionic standards was within 4% for sample concentrations higher than 1 μmol L^{-1} (~37 ppt at the STAAARTE-MED average flow rate). For lower concentrations (0.4 μmol L^{-1}, ~15 ppt), the accuracy is lower for Cl^- and NO_3^- (~10%). The repeated analysis of water samples and standard solutions indicated reproducibility within a few percent and accuracy within 10%. Blank mixing ratios are between 20 and 90 ppt for NH_4^+ and SO_4^{2-}, less than 10% of the mixing ratios in the boundary layer. For the remaining ions, blank corrections are higher, in particular for Na^+, Ca^{2+}, and Cl^- particles in the fine fraction (up to 50%).

2.2. Ground-Based Data

[13] A multifilter rotating shadowband radiometer (MFRSR-7, Yankee Environmental System, Turner Falls, MA) has been used to measure the global and the diffuse components of spectral solar irradiance (I_g and I_d respectively) simultaneously with the same detectors. This eliminates ambiguities in the comparison of the different solar irradiance components by the use of different detectors. The operating principle of the instrument is based on an automated, microprocessor-controlled shadowband, which is used to alternately shade and then expose the entrance aperture of the instrument, allowing for the measurement of the three solar radiation components. The first measurement is made with the band rotated to its nadir position (global horizontal irradiance). The diffuse component is measured by blocking the Sun disc with a metal band moving along the apparent Sun path, which can be positioned with an accuracy of 0.4° by the microprocessor-controlled stepper motor. The umbral angle defined by the metal strip is 3.27°. The diffuse measurement is made as a three-step rotation of the metal band. One measurement is made with the Sun completely blocked (diffuse irradiance on a horizontal surface) and the other two are made with the band rotated to 9° on either side of the Sun. The side measurements permit a correction for the "excess sky" that is blocked by the shadowband when the Sun-blocking measurement is made. The microprocessor then subtracts the corrected diffuse component value from the global irradiance to obtain the direct-horizontal component. Finally, the ratio of the direct-horizontal component value to the cosine of the solar zenith angle results in the value of the direct component on a surface perpendicular to the beam as

$$I_b = \frac{I_g - I_d}{\cos(\theta_0)} \tag{1}$$

where θ_0 is the solar zenith angle. The entire sequence is completed in less than 10 seconds. During STAAARTE-MED, acquisitions are stored as one-minute averages.

[14] Measurements are made over six narrowband channels (nominal wavelengths 415, 501, 615, 675, 868, and 940 nm, 10 nm full width at half maximum, FWHM) and one broadband channel (300–1100 nm). The photodiodes, interference filters, and sensitive electronic components are all held inside a temperature-controlled, desiccated enclosure. This eliminates ambient temperature-induced errors in the solar radiation data.

[15] The incident irradiance is measured on a horizontal surface constituted by a diffuser disk coupled with an integrating cavity. The response of each instrument to the radiation incident at an angle θ with respect to the surface normal (the cosine response) is measured by the manufac-

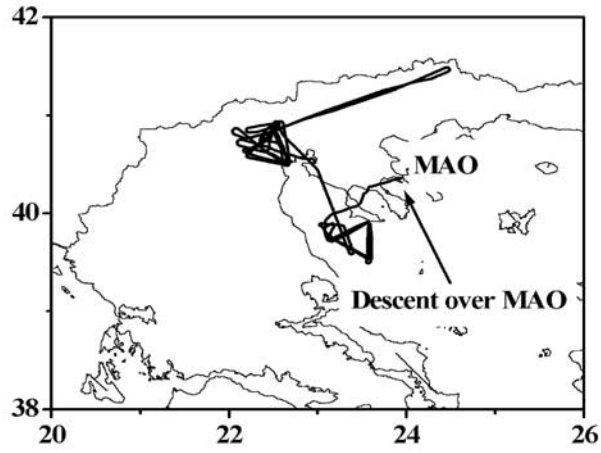

Figure 1. Flight track of flight A613 on 14 August 1998. The profile descent over MAO is also shown.

turer and supplied to the user as a correction term. The shadowband cosine response is within 8% for 0–80° zenith angle.

[16] The spectral total optical depth τ is related to the direct beam component I_b by Beer's law as

$$\tau = -\frac{1}{m}\ln\left(\frac{I_b}{I_{b0}}\right) \quad (2)$$

provided that the slant path crossed by the light (the air mass m, proportional to $(\cos(\theta_0))^{-1}$ [*Hansen and Travis*, 1974]) and the extraterrestrial irradiance I_{b0} (adjusted for the Earth-Sun distance) are known. I_{b0} can be obtained by the Langley method for clear and stable atmospheric conditions. This is rarely found at sea level. In the absence of alternative means, however, the Langley calibration was performed at the site during several days over the June–August period using the algorithm described in *Harrison and Michalsky* [1994]. The percent variation of I_{b0} is within 5% at all wavelengths, which translates in an upper limit uncertainty of τ of ±0.025 at air mass $m = 2$. For turbid conditions (as our case study), the Langley regression method cannot be applied, and instantaneous τ are calculated from Beer's law, using the average I_{b0} determined from the Langley regression. The particle optical depth τ_a is then obtained by removing the contribution of molecular extinction (Rayleigh optical depth τ_R) according to *Hansen and Travis* [1974] and gaseous absorption by O_3 from τ. Ozone correction was done using the daily averaged column amount measured by the Total Ozone Mapping Spectrometer (TOMS) instrument http://toms.gsfc.nasa.gov/index.html), equal to 310 DU on 14 August 1998).

3. Case Study of 14 August 1998

[17] The case study under consideration is a profile descent over MAO from an altitude of 4 km down to 200 m asl. The flight path is shown in Figure 1. The MAO observatory is at 170 m asl; therefore the aircraft at its lowest flight level was 30 m above the site. This particular profile has been partly discussed in previous publications [*Formenti et al.*, 2001, 2002], where it was demonstrated that the 2-km deep aerosol layer above the site was due to an aged biomass-burning plume originating from Canada. This plume extended over a large part of Europe, where it was detected clearly by multiplatform measurements [*Forster et al.*, 2001]. As a summary of the detailed discussion by *Formenti et al.* [2001, 2002], we show in Figure 2 the vertical profiles of CO and the total number of particles N_{acc} between 0.1 and 1.3 μm diameter calculated from the PCASP size distributions. A co-located layer is evident; the ratio N_{acc}/CO between 1.5 and 3 km (∼5 cm^{-3} (STP) ppb^{-1}; STP = standard temperature and pressure at p = 1013.25 hPa and T = 273 K) is typical of aged biomass burning plumes [*Andreae et al.*, 2001]. On the lower panel, Figure 2 shows the vertical profiles of the relative humidity RH and the temperature T (onboard standard instrumentation). This figure indicates a pronounced inversion just below 3.5 km altitude, particularly in the RH profile, that dropped sharply above this altitude. Below, two stable layers are evident in the temperature profile, the first below ∼1 km, the second between 1 and 3.5 km. The relative

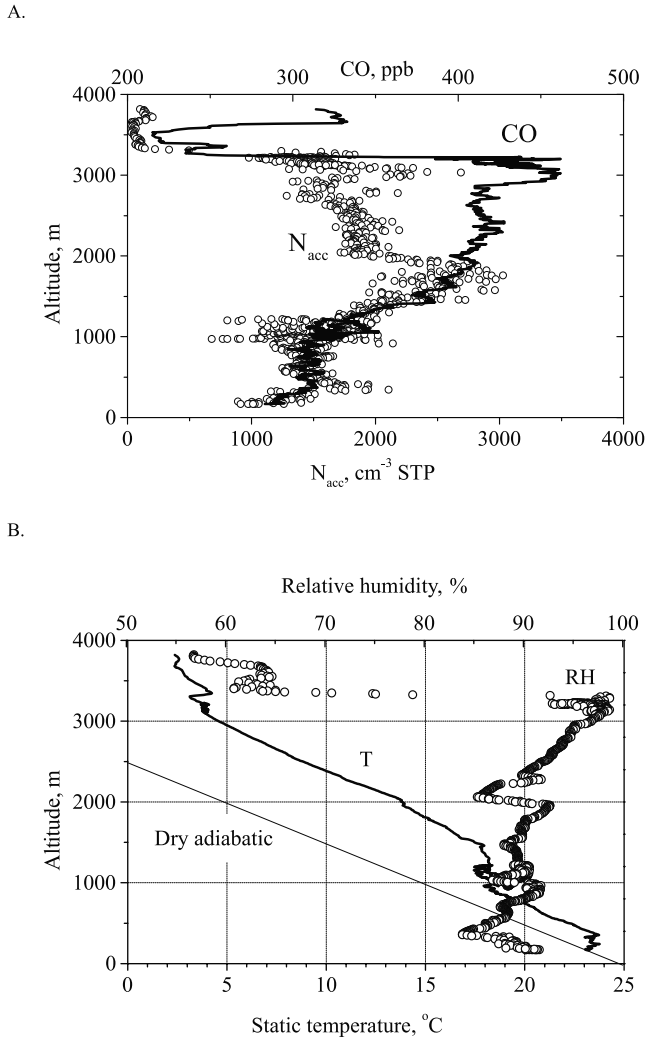

Figure 2. Vertical profiles of (a) CO and accumulation mode total particle number N_{acc} (0.1–1 μm diameter); (b) ambient static temperature and relative humidity, during the descent over MAO.

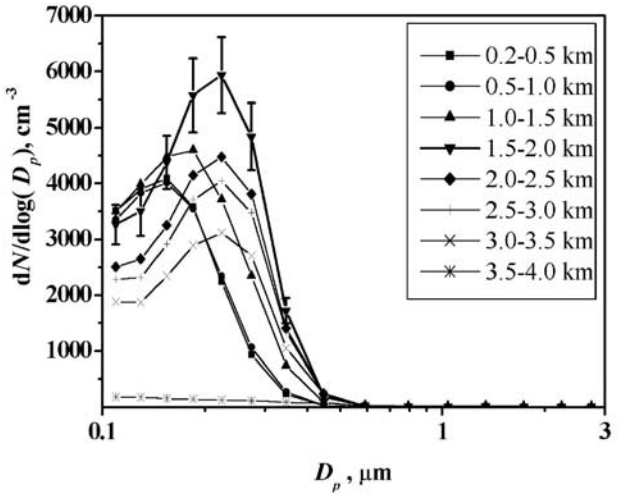

Figure 3. Aerosol size distribution (0.1–3 μm diameter) averaged over eight vertical layers (500 m deep) between 200 and 4000 m asl. For sake of clarity, error bars are shown only for the layer between 1.5 and 2 km. The error bars correspond to the total uncertainty, sum of the counting error obtained from Poisson statistics, and the standard deviation around the mean calculated for each vertical level.

humidity remained high and almost constant over these two layers, which indicates good vertical mixing.

3.1. Particle Size Distribution and Optical Parameters

[18] The particle number size distribution as a function of height is shown in Figure 3. Data have been integrated over 8 layers, each 500 m deep. Three features are evident in this plot: first, the particle concentration drops above 3.5 km. This is consistent with the vertical behavior of the tracers in Figure 2. Second, particles are almost totally concentrated in the accumulation mode, at diameters smaller than 0.5 μm; and third, there is a shift with height of the size distribution toward larger sizes. For sake of clarity, the error bars in Figure 3 are shown only for mean size distribution of the layer between 1.5 and 2 km. Error bars correspond to the total uncertainty, estimated as the root mean squared sum of the counting error obtained from Poisson statistics, and the standard deviation of the data around their mean over 500-m deep vertical layer. For all the layers, the Poisson statistic error on dN/dlogD_p stayed within 20% for particles below 0.35 μm diameter, and it was higher above. The variability over the layers was generally also within 20% for particles below 0.35 μm diameter.

[19] The accumulation mode is fitted with a lognormal size distribution as

$$\frac{dN}{d\log D_p} = \frac{N_0}{\sqrt{2\pi}\sigma}\exp\left[-\frac{1}{2}\left(\frac{\log D_p - \log \overline{D})^2}{\log^2\sigma}\right]\right. \qquad (3)$$

where N_0 is the total particle number concentration, $\overline{D}$ is the modal diameter, and σ is the geometric standard deviation.

[20] Accumulation particles in the layers between 1.5 and 3.5 km have modal diameter $\overline{D}$ of 0.19–0.20 μm (σ = 0.43), while those below 1 km have $\overline{D}$ around 0.14 μm (σ = 0.39–0.44). The layer between 1 and 1.5 km is in the transition between the two ($\overline{D}$ = 0.16 μm). The larger modal diameter in the elevated layer suggests that particles had stayed in the atmosphere a longer time and could therefore grow more than those in the boundary layer.

[21] The particle size distributions measured by the PCASP are used to calculate the dry scattering and absorption coefficients (σ_s and σ_a), which were measured independently by the nephelometer and the PSAP. We considered 100-m averages, and we used the Mie theory for spherical particles and a complex refractive index of $n = 1.55 - 0.025i$ (dry state) derived from the aerosol chemical composition. Filter measurements are not directly available for the profile. However, the horizontal uniformity of the aerosol distribution (profiles almost identical to that over MAO are detected almost 200 km away [*Formenti et al.*, 2002]), allows us to use chemical data taken elsewhere on the same flight. We used a sample taken during a straight level run at 2.3 km upwind of Thessaloniki. Based on the analysis of the filter samples, the aerosol particles are composed of sea salt, soil dust (as calcium carbonate), ammonium sulfate, black carbon (BC), and particulate organic matter (POM) [*Formenti et al.*, 2002]. Sea salt, soil dust, and ammonium sulfate are calculated from the measured Na^+, Ca^{2+}, and SO_4^{2-} concentrations. Before, Ca^{2+} and SO_4^{2-} are corrected for their sea-salt component according to *Riley and Chester* [1971].

[22] Black carbon is inferred from the absorption coefficient σ_a averaged over the length of the sampling run (16.5 ± 2.0 Mm^{-1} (STP)). The error is one standard deviation around the mean, and corresponds to a percent uncertainty of ±12%. The experimental error on σ_a is around 22% (section 2.1.3.). BC is estimated as

$$BC = \frac{\sigma_a}{\alpha} \qquad (4)$$

where α is the mass absorption efficiency. This value is set to 12.1 ± 4 m^2 g^{-1}, in accordance with the results of *Martins et al.* [1998] for biomass burning aerosols. Based on these values, the BC concentration is 1.4 μg m^{-3}, with a total uncertainty of 50%. The POM value is estimated as the difference between the total fine aerosol mass (FAM) and the sum of the mass of sea salt, soil, ammonium sulfate, and BC aerosol particles. As in the work of *Formenti et al.* [2002], the FAM at ambient relative humidity is obtained from the total fine volume (derived by integration of the PCASP size distribution) using a particle density equal to 1.14 g cm^{-3} at RH = 80% (average ambient relative humidity). The geometric growth factor $f_g(RH, RH_0)$ necessary to correct the PCASP size distribution from dry state to ambient relative humidity (average 80%) is set to 1.1. The average relative humidity inside the PCASP chamber is unknown, so the value of 30%, corresponding to the average relative humidity inside the nephelometer, is used. With these values, and considering the ±50% uncertainty of the BC concentration value, the estimated POM is 13–14 μg m^{-3}. BC accounted from 3 to 9% of the FAM, and POM for 60% to 70%. These values are in the range typical for biomass smoke [*Hobbs et al.*, 1996; *Andreae and Merlet*, 2001; *Mayol-Bracero et al.*, 2002].

[23] Assuming internal mixing of the particles, the aerosol particle refractive index $\tilde{n} = n_R - n_I i$ is calculated with

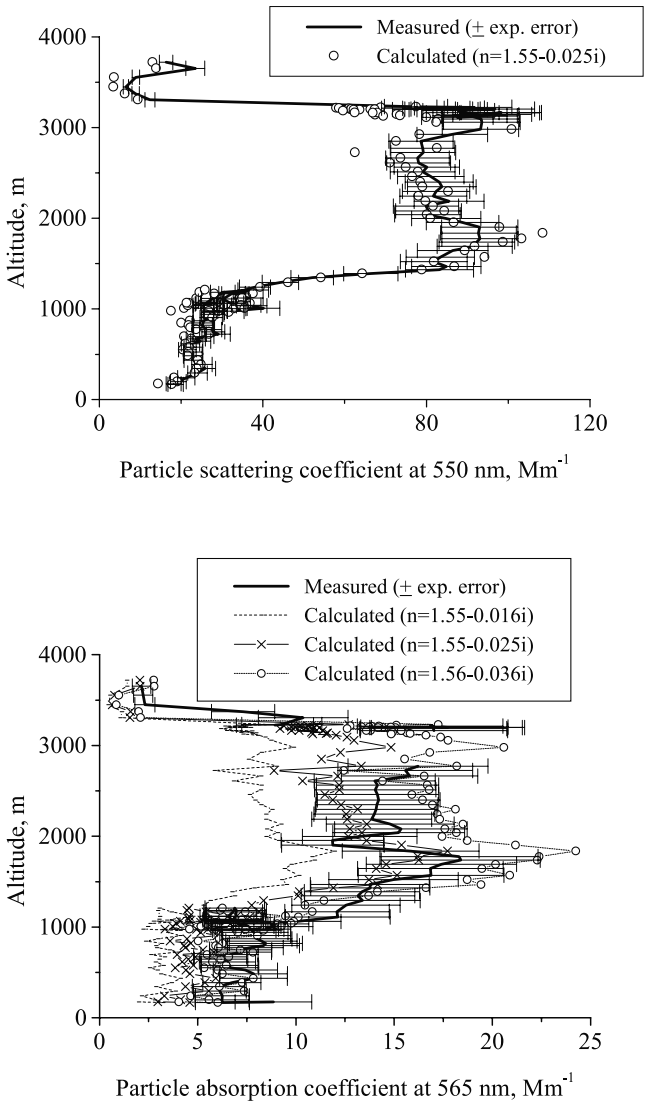

Figure 4. Vertical profile of measured and calculated (a) dry particle scattering coefficient σ_s (at 550 nm); and (b) dry particle absorption coefficient σ_a (at 565 nm). The particle scattering coefficient σ_s values measured by the nephelometer in the figure are not corrected for angular truncation and other nonidealities, while the σ_a values by the PSAP are corrected according to *Bond et al.* [1999]. Calculations are performed using the particle size distribution measured by the PCASP. The refractive index (dry state) has a central value of $\tilde{n} = 1.55 - 0.025i$, and is varied between $\tilde{n} = 1.55 - 0.016i$ and $\tilde{n} = 1.56 - 0.036i$ according to the estimated aerosol chemical composition.

the volume averaging mixing rule [see, e.g., *Horvath*, 1993]. Wavelength-dependent values of the refractive indexes for the individual components are obtained from the Optical Properties of Aerosols and Clouds (OPAC) database [*Hess et al.*, 1998] at 50% *RH* to reproduce the humidity condition of the particle size distribution, scattering, and absorption measurements. The resulting value of the complex refractive index of the mixture (at 550 nm, dry state) had a real part $n_R = 1.55$, and an imaginary part n_I ranging between 0.016 and 0.036 depending on the percentage of BC. The central value is $n_I = 0.025$. This value is in good agreement with estimates for aerosols dominated by biomass burning [*Trentmann et al.*, 2002].

[24] We compute the scattering and absorption coefficient from the PCASP size distribution and the estimated refractive index. The results of the calculations (for $\tilde{n} = 1.55 - 0.025i$) are shown in Figures 4a (scattering) and 4b (absorption). The measured scattering coefficients have not been corrected for the angular truncation, while the absorption coefficients are corrected according to *Bond et al.* [1999]. Whereas the agreement is very good for the scattering coefficient (within 10%), the calculated backscattering coefficients (not shown) are almost 50% lower than the measurements, which is in agreement with findings by *Wex et al.* [2002]. As a consequence, the measured backscatter ratio β ($\beta = \sigma_{bs}/\sigma_s$) is higher than the calculated value. This is systematically observed and points to a problem in the measurement of backscatter by the airborne nephelometer. Values of β of the order of 0.25 at 550 nm, as obtained from the measurements below 1.5 km, are extremely high compared with the literature [*Quinn et al.*, 1998; *Carrico et al.*, 1998; *Anderson et al.*, 1999; *Sheridan and Ogren*, 1999]. The comparison between σ_s and σ_{bs} measured at the lowest flight level (200 m asl) with those measured at the surface by an equivalent nephelometer shows that the airborne σ_{bs} is overestimated by about 33% (at 550 nm). The surface measurements are within 3% and 18% of the respective scattering and backscattering calculated by Mie theory. A test of sensitivity by varying the particle size distribution within the errors fails in reproducing the measured backscattering. Agreement is obtained for $n_R = 1.6$, which is not realistic for the aerosol composition measured. The error in the backscattering measurement is partly attributed to the mirror not truly truncating the scattering to between 90°–170°, but providing a linear convolved function between approximately 72° to 170° [*Anderson et al.*, 1996]. Taking this into account in the calculations allows for an increase in the backscatter ratio by 10–20% (J. Haywood, personal communication, 2001). This is not in itself enough to account for the differences. *Wex et al.* [2002] have shown that if the aerosol particles are assumed as internally mixed in calculating the refractive index, the calculated backscatter coefficients are lower by about 10% compared to the measurements.

[25] The Mie calculations for scattering and backscattering have been performed in the full (0°–180° and 90°–180°) and in the truncated (7°–170° and 90°–170°) ranges of scattering angles. Spectral correction factors C_g for the geometric truncation can thus be calculated as the ratio of full over truncated values. Due to the problems in the measurement of backscattering, we only consider the scattering coefficients. Values of C_g can be compared with the total correction factors C_t provided by *Anderson and Ogren* [1998]. *Anderson and Ogren* [1998] also provide an empirical formula to calculate C_t as a function (linear) of the scattering Ångström exponent. Our results show that C_g is of the order of 1.05 at the three wavelengths. Values of C_t range between 1.08 and 1.05 (from 450 to 700 nm). The effect of the opal glass diffuser is therefore estimated to be within 3% of the measured scattering.

[26] The results for the absorption coefficients are not independent, since the imaginary part of the refractive index

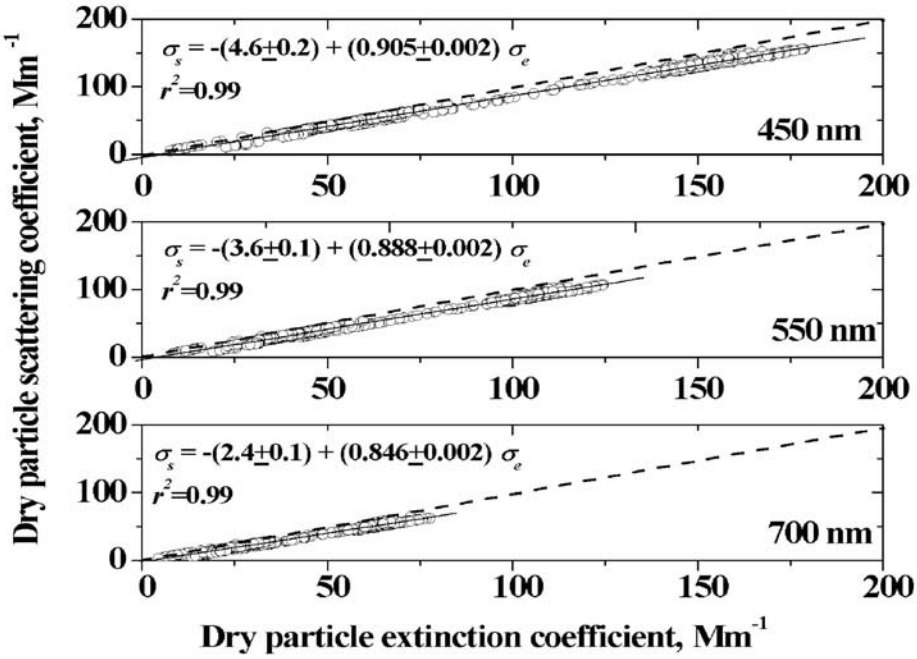

Figure 5. The dry single scattering albedo ω_0 is calculated as the slope of the linear regression of the dry particle scattering coefficient σ_s against the dry particle extinction coefficient σ_e ($\sigma_e = \sigma_s + \sigma_a$). Results are shown for 450, 550, and 700 nm. The dashed line shows the 1:1 line, corresponding to purely scattering particles.

is estimated by scaling the absorption coefficients to yield the black carbon concentration. Results suggest that a value of n_I between 0.025 and 0.036 is appropriate for the elevated aerosol layer, whereas $n_I = 0.016$ (i.e., BC = 3% of the FAM) is too low. The lower layers (<1.5 km) seem more absorbing and are well fitted by $n_I = 0.036$.

3.2. Aerosol Single Scattering Albedo

[27] To calculate the dry aerosol single scattering albedo ω_0 at 450, 550, and 700 nm, the values of measured σ_s and σ_a have been corrected for measurement artefacts using the correction factors of *Anderson and Ogren* [1998] and *Bond et al.* [1999], respectively. Spectral values of σ_a have been obtained assuming a λ^{-1}-dependence, as suggested by *Bergstrom et al.* [2002] when the absorption is due to small black carbon aerosols. This is equivalent to the assumption that the refractive index (as it is actually observed in the range 0.3–1 μm) of BC particles does not change substantially with wavelength.

[28] The single scattering albedo is calculated as the slope of the linear regression of the particle scattering coefficient σ_s against the particle extinction coefficient σ_e ($\sigma_e = \sigma_s + \sigma_a$). Results are shown in Figure 5. At all three wavelengths, the correlation is excellent ($r^2 = 0.99$). Average values are ω_0 = 0.91 (450 nm), 0.89 (550 nm), and 0.85 (700 nm), consistent with the findings of *Dubovik et al.* [2002] for urban/industrial and biomass burning aerosols. Also the spectral dependence (ω_0 is proportional to λ^2) is in agreement with *Dubovik et al.* [2002]. The decrease of ω_0 with wavelength has also been predicted by *Bergstrom et al.* [2002]. Although not obvious from Figure 5, there is a gradient in the ω_0 values between the lower (<1.5 km) and the upper layer (1.5–3 km). The elevated layer appears to be less absorbing than the lower boundary layer, where ω_0 ranges between 0.75 and 0.80. Despite being cleaner in terms of number concentration of particles, it is likely that the boundary layer is influenced by young emissions from local sources, such as vehicle exhaust, that have higher absorption efficiency.

[29] The error in ω_0 as obtained by the linear fits in Figure 5 does not take into account the experimental uncertainties on σ_s and σ_a. Formal error propagation gives

$$\frac{\delta\omega_0}{\omega_0} = (1-\omega_0)\sqrt{\left(\frac{\delta\sigma_s}{\sigma_s}\right)^2 + \left(\frac{\delta\sigma_a}{\sigma_a}\right)^2} \tag{5}$$

The percent error on ω_0 are in the range 2–6% for a range of ω_0 of 0.75 to 0.9, assuming 10% error on σ_s and 22% error on σ_a (see sections 2.1.2. and 2.1.3.).

3.3. Computation of the Aerosol Optical Depth

[30] The profiles of the spectral scattering and absorption coefficients at the three wavelengths are combined to give the aerosol optical depth $\tau_a(\lambda)$ integrated over the altitude z

$$\tau_a(\lambda) = \int_{z_1}^{z_2} [\sigma_s(\lambda, RH_0(z)) f_s(\lambda, RH(z), RH_0(z)) + \sigma_a(\lambda, RH_0(z))] dz \tag{6}$$

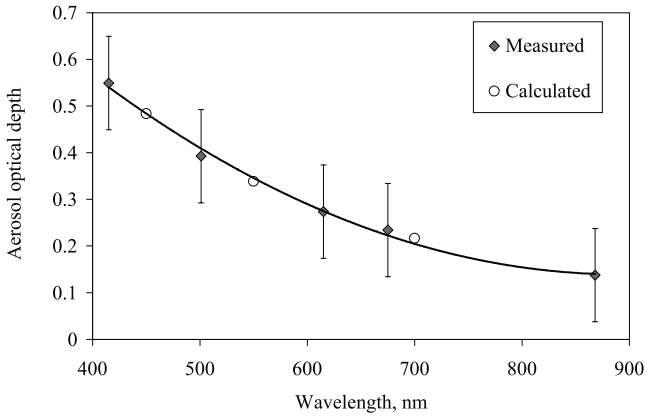

Figure 6. Comparison between the spectral aerosol optical depth measured at 13:40 UTC and those calculated from the vertical profile of the dry particle extinction coefficient σ_e ($\sigma_e = \sigma_s + \sigma_a$). Changes with humidity of the particle scattering coefficient are estimated using a scattering growth factor f_s of 1.4 ± 0.1 between 30% and 80% relative humidity.

[31] At every wavelength, the dependence of the scattering coefficient on the ambient relative humidity (RH) and the sampling relative humidity (RH_0, inside the nephelometer chamber) is made explicit by the scattering growth factor $f_s(\lambda, RH, RH_0)$, which we assumed in the form

$$f_s(\lambda, RH, RH_0) = \left(\frac{1 - RH/100}{1 - RH_0/100}\right)^{-\gamma} \quad (7)$$

The functional dependence of $f_s(\lambda, RH, RH_0)$ via the γ-parameter is given according to *Hänel* [1976]. As specific data are not available, the absorption coefficient is considered as independent of humidity. Previous studies have considered this dependence, and empirically constrained the absorption growth factor to vary between 1 and the scattering growth factor [*Hartley et al.*, 2000]. The comparison between the τ_a values measured at the ground and those calculated via equation (6) has been discussed by *Formenti et al.* [2002], where a discussion of the associated uncertainties is included. The scattering growth factor is treated as a free parameter. For that, the value of γ at each of the 450, 550, and 700 nm wavelengths is varied until the calculated aerosol optical depth is in agreement (within 2%) with the experimental value extrapolated according to the spectral dependence of the measured aerosol optical depth. In this approach, the effect of aerosol particles above 4 km altitude is neglected. Also, it is implicitly assumed that particles above 1 μm diameter (the approximate cutoff of the nephelometer and the PSAP) do not contribute to light extinction. This is confirmed by inspecting the curves of the surface size distributions $dS/d\log D_p = \pi D_p^2 dN/d\log D_p$, that virtually drop to zero above 1 μm diameter.

[32] The results of the computation of equation (6) are shown in Figure 6, where a second order polynomial is fitted through the measured and the calculated data to indicate that the spectral dependence of the τ_a values is consistent between the two data sets. The reference values of τ_a used as term of comparison for the calculated τ_a have been interpolated to 450, 550, and 700 nm from the shadowband measurements using an Ångström exponent of 1.86 ± 0.04 (first-order fit of ln (τ_a) versus ln (λ), r^2 = 0.99). The column average for $f_s(\lambda = 550$ nm, $RH = 80\%$, $RH_0 = 30\%)$ used for the data in Figure 6 is 1.4 ± 0.1. *Kotchenruther and Hobbs* [1998] measured an average f_s for biomass burning aerosols above the Amazon Basin of 1.16 ($\lambda = 550$ nm, $RH = 80\%$, $RH_0 = 30\%$), and f_s is in the range 1.4–2.7 for anthropogenic aerosols [*Kotchenruther et al.*, 1999]. The lowest value is attained when the carbon mass content is highest. Assuming that the most likely estimate of f_s lies in the range 1.16-1.4 means that the particle extinction optical depth (obtained as the sum of the vertically integrated particle scattering and absorption coefficients) obtained from the aircraft measurements over the altitude range of 200 to 4000 m asl represents between 70% and 100% of the aerosol optical depth measured by the ground-based shadowband, and that the atmosphere above 4000 m asl contributes less <30% to the total τ_a.

4. Radiative Transfer Calculation

4.1. Model Structure and Initialization

[33] The global, diffuse, and direct downwelling irradiances at the surface are calculated using the Streamer radiative transfer model [*Key*, 2001]. The radiative transfer equation is solved by the "discrete ordinate" method over 24 short-wave bands. Gaseous absorption is determined with the exponential-sum fitting of transmissions technique. Only gases with significant absorption (water vapor, oxygen, carbon dioxide, and ozone) are included using data by *Tsay et al.* [1989]. The extraterrestrial irradiances used in Streamer are compiled from MODTRAN3. The total solar irradiance in the shortwave spectrum (0.28–4.0 μm) is 1354.2 W m^{-2}. This value is based on the mean Earth-Sun distance, and differs from the typical "solar constant" value of approximately 1370 W m^{-2} (at a mean Earth-Sun distance) because of the difference in the width of the solar spectrum. From 0.2 to 5.0 μm, the Streamer total solar flux is approximately 1367 W m^{-2}.

[34] In this study we do not use the aerosol models defined in Streamer but rather prescribe our own spectrally independent aerosol models [*Boucher et al.*, 1998]. In our calculation, the dry particle size distributions measured as a function of height are averaged over 500-m thick layers from sea level up to 4 km, and used to calculate the ambient particle optical properties (extinction coefficients, single scattering albedo, and asymmetry factor) by Mie theory. As in section 3.1, dry particles are grown to ambient humidity assuming that the particle diameters at ambient and at a reference low relative humidity (D_p and D_{p0}, respectively at RH and RH_0) are related as

$$D_p = D_{p0}\left(\frac{1 - RH/100}{1 - RH_0/100}\right)^{-\gamma'} = D_{p0} f_g(RH, RH_0) \quad (8)$$

The mean ambient relative humidity RH at the vertical levels is obtained from aircraft data. Because the relative humidity inside the PCASP chamber is unknown, the RH_0 is fixed to 30%, corresponding to the average relative humidity inside the nephelometer. Equation (8) is based on

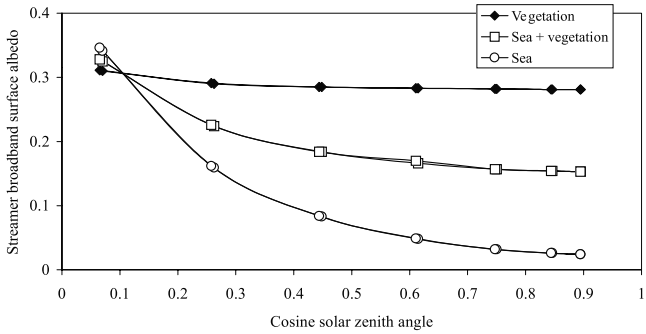

Figure 7. The broadband surface albedo as a function of the solar zenith angle as obtained by Streamer for vegetation, sea plus vegetation, and sea surfaces. The parameterization of the wavelength-independent sea surface albedo by *Glew et al.* [1998] is shown for comparison.

the growth model of *Hänel* [1976], under the assumption that scattering is proportional to the particle volume. Under this assumption $\gamma' = \gamma/3$ and $f_g = f_g^{1/3}$. Changes with humidity of the aerosol refractive index are considered with the volume-mixing rule assuming that the dry fraction of the aerosol (with refractive index $\tilde{n}_d = n_{Rd} - n_{Id}i = 1.55 - 0.025i$ is mixed with water (refractive index $\tilde{n}_w = 1.33 - 0.0i$) to give the total ambient aerosol volume with refractive index $\tilde{n} = n_R - n_I i$

$$n_R = 1.33 + (n_{Rd} - 1.33)\left(\frac{D_{p0}}{D_p}\right)^3$$
$$n_I = n_{Id}\left(\frac{D_{p0}}{D_p}\right)^3 \quad (9)$$

[35] The value of γ' is adjusted so that the aerosol optical depth calculated by the off-line Mie program matches the measured optical depth at 501 nm. Differently to the scattering growth factor in section 3.3, the spectral variations of the geometric growth factor f_g are not considered, that is, the ''best fit'' value of f_g obtained at 501 nm is used at the remaining wavelengths. These are: $\gamma' = 0.063$ for $\tilde{n}_d = 1.55 - 0.025i$ (corresponding to $f_g(RH = 80\%, RH_0 = 30\%) \sim 1.1$ and $f_s(\lambda = 501$ nm, $RH = 80\%, RH_0 = 30\%) \sim 1.3$), and $\gamma' = 0.057$ for $\tilde{n}_d = 1.56 - 0.036i$ ($f_g(RH = 80\%, RH_0 = 30\%) \sim 1.1$ and $f_s(\lambda = 501$ nm, $RH = 80\%, RH_0 = 30\%) \sim 1.2$). These values are in good agreement with the average value of $f_s(\lambda = 550$ nm, $RH = 80\%, RH_0 = 30\%)$ obtained in section 3.3 assuming the same functional dependence of aerosol scattering on humidity, but altitude-dependent values of the reference humidity RH_0.

[36] Differences due to the assumptions on the spectral dependence of the growth factors should be negligible due to the weak variations obtained for $f_s(\lambda, RH, RH_0)$ between 450 and 700 nm (1.4 to 1.5) [*Formenti et al.*, 2002]. The large uncertainties on these values, however, inhibit further conclusions.

[37] The ambient spectral extinction coefficients, single scattering albedo, and asymmetry factors calculated by the Mie code from the two aerosol models are used as input parameters for Streamer. The vertical profiles for pressure, temperature, ozone, and water vapor are chosen as the standard midlatitude summer profiles [*McClatchey et al.*, 1971]. As MAO is located on a narrow strip of land (~30 km wide) overlooking the sea, the surface albedo is initially set as a mixture of open seawater (50%) and vegetation (50%), and then varied to seawater only and vegetation only. The curves corresponding to the various surface types are shown in Figure 7. Note that the differences between the sea surface albedo model in Streamer (using data from *Briegleb et al.* [1986]) and the unpublished data of M. Glew et al. (unpublished data, 1998; hereinafter referred to as Glew et al. [1998]), which was used for the radiative transfer calculations of *Russell et al.* [1999] and *Redemann et al.* [2000] might be as large as 63% at low solar elevation. As the sea surface albedo depends critically on the wind speed, comparing different models is not meaningful *in se*. However, it is interesting to see how the choice of a different albedo model would influence the results of model calculations of the diffuse and global irradiances, and take this effect into account when comparing results from various model calculations. The solar zenith angle is calculated from the geographical latitude and longitude and UTC time. This parameter is also varied by ±1 degree to test the sensitivity to errors in the experimental settings of the shadowband (misleveling of the horizontal diffuser, or wrong UTC time or geographical location settings). This represents an upper bound of the actual uncertainty for this parameter. As an example, one-degree error on the solar zenith angle corresponds, at the maximum, to a one-minute error in the time setting at MAO on 14 August 1998, which is excessive taking into account the care with which the instrument was operated and the precision of the global positioning system (GPS) used to synchronize the instrument clock. Finally, the input aerosol size distribution varies due to the experimental error according to the Poisson counting statistic (equal to the square root of the measured counts in each size bin) and to the dispersion of the values around their mean on each flight level. Below 0.5 μm diameter (where most of the particles are found), these variations are within 30% and can be compensated by varying the γ'-parameter (i.e., the geometric growth factor) to reproduce the measured aerosol optical depth. No sensitivity study regarding the size distribution is therefore performed. The sensitivity to the aerosol chemical composition is tested by varying the dry refractive index from $\tilde{n} = 1.55 - 0.025i$ to $\tilde{n} = 1.56 - 0.036i$. In Figure 8 the vertical ambient particle extinction coefficient, single scattering albedo, and backscatter fraction calculated by the Mie code at 501 nm are compared to the corresponding measurements by the airborne nephelometer and PSAP at 450 and 550 nm. Because of the problem with the particle backscattering coefficient measurements (section 3.1), the comparison for the backscatter ratio is not shown. Differences between the model calculations (estimated as (1 – calculation ($\tilde{n} = 1.56 - 0.036i$)/calculation ($\tilde{n} = 1.55 - 0.025i$)) × 100) are within 2% for the particle extinction coefficient, within 5% for the single scattering albedo, and within 3% for the particle backscatter ratio.

4.2. Computation of the Spectral Downwelling Irradiances

[38] To obtain spectral irradiances in units of W m^{-2} nm^{-1}, the actual measurements (in Volts or counts) are converted using the Langley-extrapolated calibration coef-

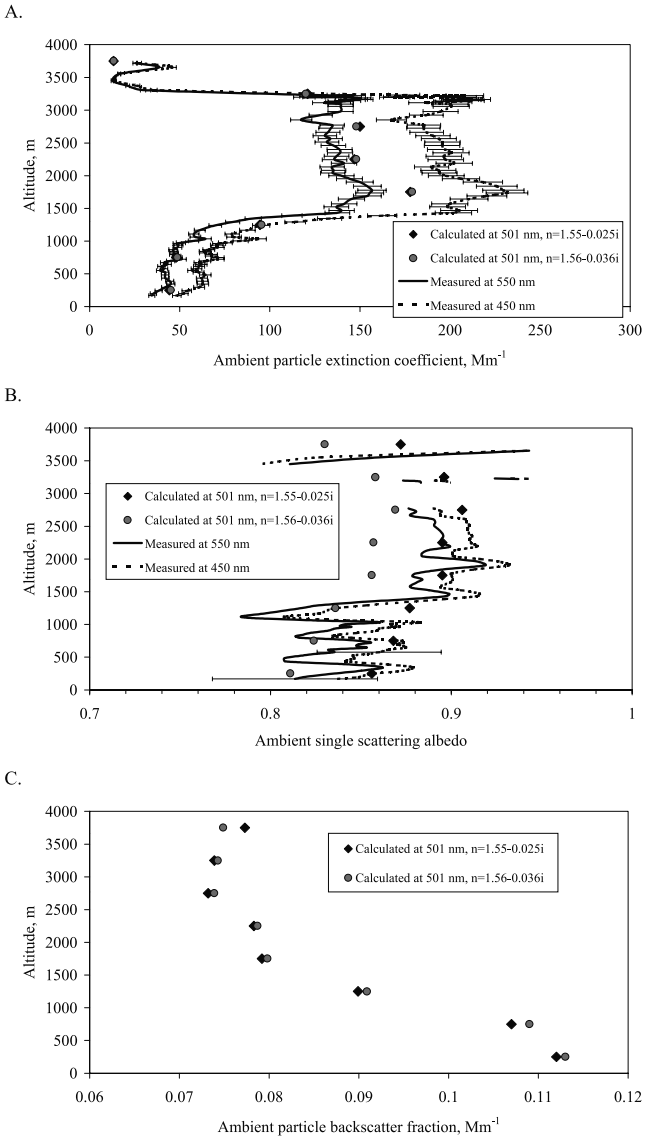

Figure 8. Comparisons of (a) the ambient aerosol extinction coefficients at 501 nm; (b) the ambient single scattering albedos at 501 nm; and (c) the ambient backscatter ratios at 501 nm calculated for the two aerosol models by the off-line Mie program input of the Streamer radiative transfer code with their counterparts measured by the airborne nephelometer and PSAP at 450 and 550 nm. Only in the case (c) comparison with experimental data is not shown.

ficients (also in Volt or count units) and the spectral solar irradiance data at the top of the atmosphere. However, because the Langley calibration of the shadowband done at sea level is prone to large uncertainties, and because the instrument was calibrated by the manufacturer only few months before the installation at the site, we choose in alternative to use the manufacturer's calibration to transform the Langley-extrapolated voltages on clear-days to solar irradiances and then compare those to the values tabulated by *Thakaekara* [1992]. The solar spectrum of *Thakaekara* [1992] is equivalent to that of Streamer in practical terms. With this choice, the Langley calibration becomes useless to calculate the actual irradiance values, but the ratio of the experimentally extrapolated spectral solar irradiance (W m^{-2} nm^{-1}) to reference values provides, in the absence of alternative means, an upper limit to the uncertainty on the irradiance measurements. We only retained wavelengths for which the ratio between the measured and tabulated spectral irradiances was within 5%. This criterion was met at 415, 501, and 615 nm, for which the direct and diffuse downwelling irradiances are computed.

[39] Results of the computation at 13:40 UTC (time of overflight) are shown in Figure 9 for the aerosol optical depth and the irradiance at 501 nm. The measured irradiance values have been integrated over the filter passbands of the shadowband to be comparable with the values calculated by Streamer (in W m^{-2}). As expected, the measured and calculated values agree (within 0.007 τ_a units, corresponding to 2% = (1 – calculation/measurement)

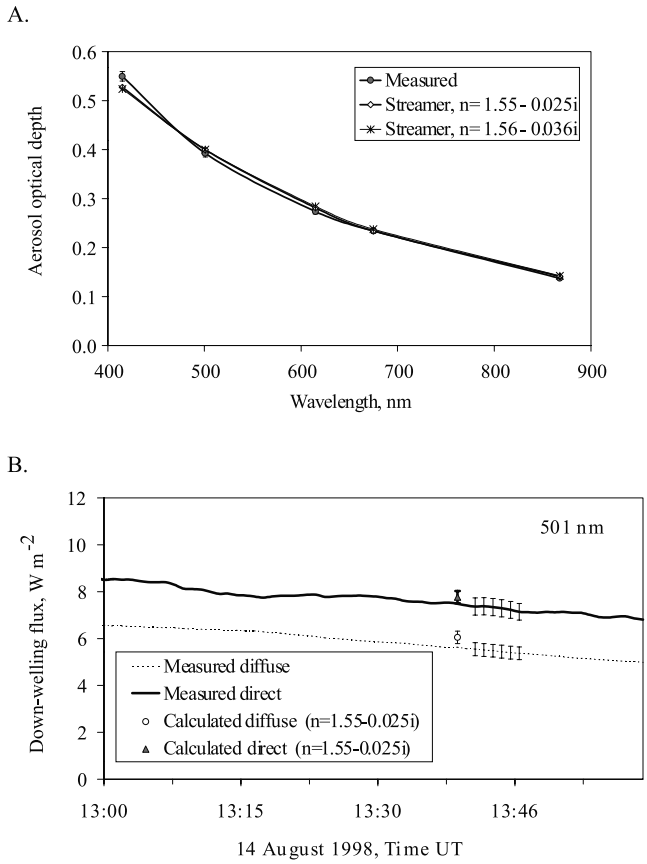

Figure 9. Comparison of the (a) ambient spectral aerosol optical depth and (b) downwelling direct and diffuse irradiances (W m^{-2}) at 501 nm at 13:40 UTC with the counterparts calculated by Streamer. The errors on the measured aerosol optical depths correspond to the measurement uncertainties, but they are not graphically visible. The error bars on the measured irradiances correspond to a 5% uncertainty. The Streamer input size distribution has a vertical resolution of 500 m over eight vertical layers (Figure 3). The refractive indexes are set to $\tilde{n} = 1.55 - 0.025i$ and $\tilde{n} = 1.56 - 0.036i$ (dry state).

Table 1. Comparison of the Measured and Modeled Direct and Diffuse Irradiance at 13:40 UTC

	Measured	Calculated	(1-Calc./Meas.) × 100
		Direct, W m^{-2}	
415 nm	4.3 ± 0.2	4.6 ± 0.2	−7%
501 nm	7.37 ± 0.07	7.8 ± 0.3	−5%
615 nm	9.07 ± 0.09	9.56 ± 0.03	−6%
		Diffuse, W m^{-2}	
415 nm	6.0 ± 0.3	6.5 ± 0.3	−7%
501 nm	5.54 ± 0.06	6.1 ± 0.3	−9%
615 nm	3.73 ± 0.04	4.2 ± 0.2	−12%

× 100) at 501 nm. There is also a good agreement (within 3%) at the other wavelengths. The measured and calculated Ångström exponents agree within 4%. This means that, by adjusting the response to the relative humidity, and by including into this adjustment any remaining uncertainty, we can reproduce the spectral dependence of the measured τ_a using the PCASP particle size distribution (corrected for ambient *RH*) and a wavelength-independent refractive index.

[40] The discrepancy between the modeled and measured spectral direct irradiances (see Table 1 for values) is of the order of 5–7%. The calculated irradiances are higher than the measurements independently of whether the calculated aerosol optical depths are higher (as at 501 and 615 nm), or lower (as at 415 nm) than the measurements. The discrepancy δF between the calculated and the measured direct irradiances (F_c and F_m, respectively) can be written as

$$\delta F = 1 - \frac{F_c}{F_m} = e^{-\delta\tau_a m} \tag{10}$$

where $\delta\tau_a = \tau_{a,c} - \tau_{a,m}$ is the difference between the calculated and the measured aerosol optical depths, and m is the air mass. For the air mass of 1.5 (corresponding to the mean zenith angle at the time of overpass), δF corresponds at the most to − 4%. The sensitivity of the direct irradiance to the aerosol vertical profiles has been investigated previously and not found to be critical in the absence of clouds (O. Boucher, unpublished results, 2000). As discussed in section 4.1, the one standard deviation errors on the modeled irradiances are estimated as the sum of the (1) uncertainties in the refractive index; (2) uncertainties in the surface albedo; and (3) uncertainties in the solar zenith angle. The individual contributions to the overall uncertainty are shown in Table 2. The total uncertainty on the modeled irradiances is equal to the root-squared sum of the squares of the individual errors. The effect of changes in the surface albedo, the solar zenith angle, and the refractive index are within 5% at all wavelengths and for both the direct and diffuse components. The refractive index has the larger effect on the diffuse component. In Figure 9, the 5% error bars for the measured irradiances are also indicated. Within one standard deviation (estimated as the square root of the sum of the measurement and calculations errors, both squared), the calculated direct irradiance at 501 nm is compatible with the measurements, while the calculated diffuse irradiance is higher than the measurements and it is not consistent with it. At 415 and 615 nm, both the calculated direct and the diffuse irradiances are 5% to 12% higher than the measurements and not consistent with them within one standard deviation. The reason for these discrepancies is not investigated further, however, it is likely to be largely due to calibration of the flux measurements.

4.3. Shortwave Direct Clear-Sky Aerosol Forcing

[41] The average dry particle size distribution sampled at 13:40 UTC is used to calculate the diurnal cycle of the global solar irradiance (downwelling and upwelling) between 280 and 4000 nm. This is the spectral interval where most of the solar radiation is found [*Iqbal*, 1983]. The extrapolation of the particle size distribution at 13:40 UTC to the entire day is justified by the fact that the Ångström exponent calculated from the spectral aerosol optical depth has only 3% variation during the whole day (1.81 ± 0.05 between 415 and 868 nm). The dry refractive indexes and humidity response correspond to the previous aerosol models ($\tilde{n} = 1.55 - 0.025i$, $\gamma = 0.19$; and $\tilde{n} = 1.56 - 0.036i$, $\gamma = 0.17$). The critical assumption in this case is that it is possible to extrapolate the two aerosol models from the visible and near-infrared region (415–868 nm) to the entire solar spectrum. This applies both for the particle size distribution, which was measured only up to 3-μm diameter, and therefore provides information on light extinction only at wavelengths below 1.5–2 μm, and for the refractive index, which was assumed to be constant with wavelength. Again this can be a reasonable approximation for wavelengths below 2.5 μm [*Russell et al.*, 1999; *Redemann et al.*, 2000], but not above. As a consequence, the irradiance calculations are subject to substantial uncertainty.

[42] We calculate the direct clear-sky shortwave aerosol radiative forcing at the surface and at the top of the atmosphere (TOA) as the difference between the net irradiances (downwelling minus upwelling) when aerosols are considered and those when aerosols are absent, keeping fixed the atmospheric conditions (vertical profiles, molecular scattering and absorption, surface albedo, solar zenith

Table 2. Percent Errors for the Model Calculation of the Direct and Diffuse Irradiances Done for 13:40 UTC, Time of Overpass of the Surface Site MAO[a]

	415 nm	501 nm	615 nm
	Direct, W m^{-2}		
Surface albedo	0%	0%	0%
Solar zenith angle	4.2%	3.4%	2.9%
Refractive index	0.5%	0.1%	0.4%
Total	4.2%	3.4%	2.9%
	Diffuse, W m^{-2}		
Surface albedo	0.8%	1.2%	1.9%
Solar zenith angle	1.4%	1.2%	1.0%
Refractive index	4%	4%	4%
Total	4.4%	4.4%	4.4%

[a] Percent variations are given with respect to the base case of the following: input dry size distribution averaged over 500-m layers starting from the surface up to 4 km; refractive index $\tilde{n} = 1.55 - 0.025i$; surface as a mixture of open seawater (50%) and vegetation (50%); solar zenith angle of 48°44′ (calculated from the latitude and longitude MAO and the time of overpass (13:40 UTC)). The following sensitivity tests have been performed: (1) surface albedo: the surface model is varied to pure seawater and pure vegetation; (2) solar zenith angle: the solar zenith angle is varied of ±1 degree; (3) refractive index: the refractive index is varied to $\tilde{n} = 1.56 - 0.036i$. The physical significance of these variations is discussed in the text.

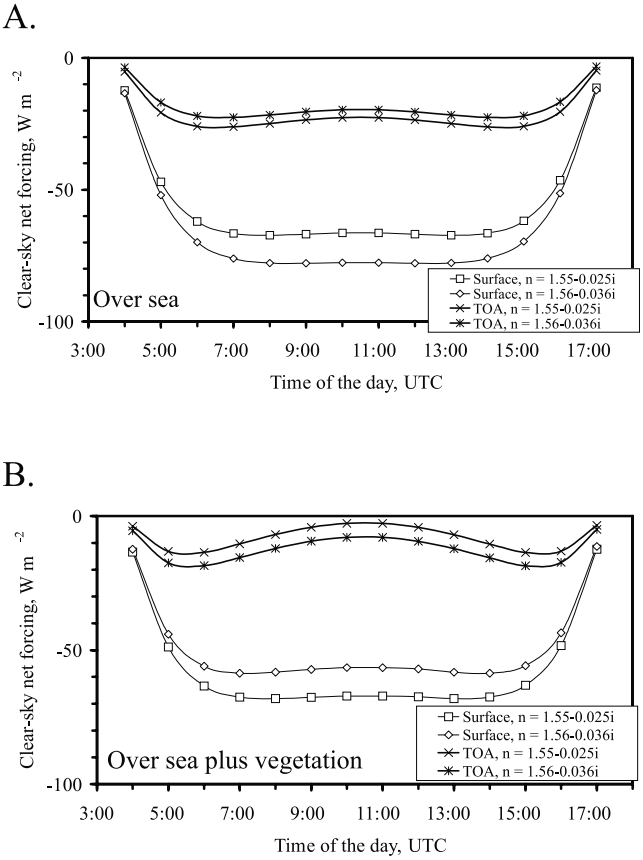

Figure 10. The net direct clear-sky short-wave aerosol forcing (280–4000 nm) predicted by the two aerosol models over MAO ($\tilde{n} = 1.55 - 0.025i$ and $\tilde{n} = 1.56 - 0.036i$) is shown at the top of the atmosphere (TOA) and at the Earth's surface (a) over the sea surface and (b) over the "sea plus vegetation" surface.

angle). The idea is to estimate the effect of the two experimentally determined aerosol models on the radiation budget of the eastern Mediterranean. Midvisible aerosol optical depth values of the order of 0.3–0.4 are not uncommon in the area [*Formenti et al.*, 2002] (see also the AERONET web site http://aeronet.gsfc.nasa.gov/); therefore, the results of this case study have a broad applicability.

[43] We considered two surface types as (1) open seawater or (2) open seawater plus vegetation (Figure 7). The vertical profiles are chosen as in section 4.1. The diurnal cycles are shown in Figure 10, while the corresponding daytime averages are reported in Table 3. The aerosol forcing is negative (net cooling), and, due to absorption, much higher at the surface (up to – 78 W m^{-2}) than at the TOA (forcing up to – 26 W m^{-2}). This effect is more pronounced over the sea than over the mixture sea/vegetation surface. The well-known minimum of the aerosol forcing at the TOA around solar noon is at the contrary more pronounced for the sea/vegetation than for the sea-only surface. Differences between the two models (due to changes in the aerosol refractive index) are in the range 9–17% at the surface, and 13–33% at the TOA. The variations are lowest at large zenith angles for the surface, but highest at the TOA.

5. Conclusions

[44] The "closure" tests on the aerosol measurements (airborne and ground-based) of the forest-fire haze layer above MAO have shown that, within the experimental errors, there is an internal consistency amongst the collected data. Major uncertainties are in the determination of the carbonaceous fraction of the aerosol mass (organic and black carbon), which was not measured directly but estimated indirectly from measurements of the aerosol absorption and the total volume. Black carbon has been considered as the only strong aerosol absorber, although substantial absorbing components in biomass smoke could be organic compounds that would not have the optical properties of graphite-like "black carbon" [*Mukai and Ambe*, 1986]. Within the aerosol layer, black carbon accounts for 6–9% of the total accumulation mode mass (ambient state). Furthermore, the particle refractive index (and in particular, its imaginary part) is set as wavelength-independent. This assumption appears reasonable as it allows reproducing the measured spectral aerosol optical depth from the measured aerosol size distribution (to within 3%).

[45] The response of scattering to changes in the atmospheric relative humidity is also estimated from the closure calculations. The aerosol absorption is considered as independent of humidity, while the humidity growth factor for scattering is constrained by the requirement that the measured ambient extinction (sum of scattering and absorption) reproduces the total column extinction measured from the ground. Although in absolute terms this can be a significant source of error, in practice leaving the scattering growth as a free parameter permits to compensate for errors in the determination of the aerosol size distribution when the aerosol optical depth is calculated in the radiative transfer code.

[46] Using the measured aerosol size distribution and the estimated refractive index as input parameters, the modeled and measured irradiances agree within three standard deviations, with the tendency for the diffuse irradiance to be overestimated by the model to a greater extent than the direct component. The possibility of a systematic overestimation of the diffuse irradiance by models, particularly at low altitude sites, is a controversial issue, as several case

Table 3. Daytime Averages of the Clear-Sky Net Radiative Aerosol Shortwave Forcing (280–4000 nm) at the Surface and at the Top of the Atmosphere (TOA) Estimated for the Two Aerosol Models[a]

Refractive Index	Surface, W m^{-2}	TOA, W m^{-2}	Ratio Surface/TOA
	Sea Surface		
$\tilde{n} = 1.55 - 0.025i$	−55 (±20)	−21 (±7)	2.6
$\tilde{n} = 1.56 - 0.036i$	−63 (±23)	−18 (±6)	3.5
	Sea Plus Vegetation		
$\tilde{n} = 1.55 - 0.025i$	−49 (±16)	−12 (±5)	4.0
$\tilde{n} = 1.56 - 0.036i$	−56 (±20)	−8 (±4)	7.2

[a] Measured dry size distribution averaged over 500-m layers starting from the surface up to 4 km; refractive indexes $\tilde{n} = 1.55 - 0.025i$ and $\tilde{n} = 1.56 - 0.036i$. The underlying surface is chosen as open seawater, or as a mixture of open seawater (50%) and vegetation (50%). Standard deviations around the means are in parentheses.

studies indicating either agreement or discrepancy between modeled and measured surface irradiances are found in the literature [*Halthore*, 1999; *Satheesh and Ramanathan*, 2000; *Wendisch et al.*, 2002].

[47] The estimated daytime average clear-sky net short-wave forcing at the TOA is between −18 and −21 W m^{-2} (over sea) depending on the refractive index of the aerosol model. The influence of the surface albedo is extremely large, and the forcing decreases up to a factor of two by passing from the sea to the sea plus vegetation surface. Differences due to the choice of the aerosol model, that is, the imaginary part of the refractive index, are around 10% above sea, but around 32% (±16% standard deviation) above the ''sea plus vegetation'' surface. This is in agreement with conclusions of *Redemann et al.* [2000] for aerosols with imaginary part larger than 0.01. *Redemann et al.* [2000] estimate a net TOA cooling of about 39 W m^{-2} (in the range 0.2–4 μm) for an aerosol with ambient $\omega_0 \sim 0.95$ (at 550 nm) and $\tau_a \sim 0.7$ at 450 nm, therefore more scattering and less absorbing than the aerosol layer encountered on 14 August 1998. Using a different sea surface albedo induces a change in short-wave forcing of 0.5% for a zenith angle of 52°, where the difference between the Streamer sea surface model and the data of Glew et al. [1998] are minimal (∼7%), up to 46% at 86° zenith angle, where the differences between the two models are of the order of 63%.

[48] The aerosol effect is very significant for the surface radiative forcing, where the daytime averaged net forcing (still negative) is estimated to be within 55 and 63 W m^{-2} (above sea). The influence of the surface albedo is of the order of 13% (lower net forcing above sea plus vegetation). The STAAARTE-MED ratio between the surface forcing and the TOA forcing above the sea is of about 3, consistent with results of the Indian Ocean Experiment (INDOEX) for a single scattering albedo of 0.89 at 670 nm [*Satheesh and Ramanathan*, 2000; O. Boucher, unpublished results, 2001]. While, as noted by *Boucher and Tanré* [2000], increasing the aerosol absorption decreases the aerosol effect at the TOA, the surface forcing is enhanced when the aerosol absorption is larger. In our case, changing the imaginary part of the refractive index from 0.025 to 0.036 (corresponding to 6% and 9% black carbon by mass, respectively) increases the surface forcing by about 10% independently of the surface type, and reduces the TOA forcing by about 11%. For a less absorbing aerosol particles, *Redemann et al.* [2000] estimated a ratio surface/TOA around 1.4. The redistribution of energy within the atmosphere due to the vertical asymmetry of the aerosol forcing might affect cloud convection, and reduce the evaporation of water from the sea surface.

[49] **Acknowledgments.** This research was financially supported by the Max Planck Society, Germany. The STAAARTE project, using MRF and the C-130 aircraft facility, has been funded by the European Commission through the TMR (Training and Mobility of Researchers), Access to Large Scale Facilities Programme, contract ERBFMGECT950069. The air and ground crews, and the observers of the Meteorological Research Flight, deserve appreciation for the serious professionalism, yet the pleasantness, of their work environment. R. Gabriel (MPIC) assisted with the IC analysis.

References

Anderson, T. L., and J. A. Ogren, Determining aerosol radiative properties using the TSI 3563 integrating nephelometer, *Aerosol Sci. Technol.*, *29*, 57–69, 1998.

Anderson, T. L., et al., Performance characteristics of a high-sensitivity, three-wavelength, total scatter/backscatter nephelometer, *J. Atmos. Oceanic Technol.*, *13*, 967–986, 1996.

Anderson, T. L., D. S. Covert, J. D. Wheeler, J. M. Harris, K. D. Perry, B. E. Trost, D. J. Jaffe, and J. A. Ogren, Aerosol backscatter fraction and single scattering albedo: Measured values and uncertainties at a coastal station in the Pacific Northwest, *J. Geophys. Res.*, *104*, 26,793–26,807, 1999.

Andreae, M. O., and P. Merlet, Emission of trace gases and aerosols from biomass burning, *Global Biogeochem. Cycles*, *15*, 955–966, 2001.

Andreae, M. O., W. Elbert, R. Gabriel, D. W. Johnson, S. Osborne, and R. Wood, Soluble ion chemistry of the atmospheric aerosol and SO_2 concentrations over the eastern North Atlantic during ACE-2, *Tellus, Ser. B*, *52*, 1066–1087, 2000.

Andreae, M. O., et al., Transport of biomass burning smoke to the upper troposphere by deep convection in the equatorial region, *Geophys. Res. Lett.*, *28*, 951–954, 2001.

Ansmann, A., U. Wandinger, A. Wiedensohler, and U. Leiterer, Linderberg Aerosol Characterization Experiment 1998 (LACE 98): Overview, *J. Geophys. Res.*, *107*, doi:10.1029/2000JD000233, in press, 2002.

Bergstrom, R. W., P. B. Russell, and P. Hignett, On the wavelength dependence of the absorption of black carbon particles: Predictions and results from the TARFOX experiment and implications for the single scattering albedo, *J. Atmos. Sci.*, *59*, 567–577, 2002.

Bond, T. C., T. L. Anderson, and D. Campbell, Calibration and intercomparison of filter-based measurements of visible light absorption by aerosols, *Aerosol Sci. Technol.*, *30*, 582–600, 1999.

Boucher, O., and D. Tanré, Estimation of the aerosol perturbation to the Earth's radiative budget over oceans using POLDER satellite aerosol retrievals, *Geophys. Res. Lett.*, *27*, 1103–1106, 2000.

Boucher, O., et al., Intercomparison of models representing shortwave radiative forcing by sulfate aerosols, *J. Geophys. Res.*, *103*, 16,979–16,998, 1998.

Briegleb, B. P., P. Minnis, V. Ramanathan, and E. Harrison, Comparison of regional clear-sky albedos inferred from satellite observations and model computations, *J. Clim. Appl. Meteorol.*, *25*, 214–226, 1986.

Carrico, C. M., M. J. Rood, and J. A. Ogren, Aerosol light scattering properties at Cape Grim, Tasmania, during the First Aerosol Characterization Experiment (ACE1), *J. Geophys. Res.*, *103*, 16,565–16,574, 1998.

Collins, D. R., et al., In situ aerosol-size distributions and clear-column radiative closure during ACE-2, *Tellus, Ser. B*, *52*, 498–525, 2000.

Dubovik, O., B. N. Holben, T. F. Eck, A. Smirnov, Y. J. Kaufman, M. D. King, D. Tanré, and I. Slutsker, Variability of absorption and optical properties of key aerosol types observed in worldwide locations, *J. Atmos. Sci.*, *59*, 609–619, 2002.

Eisinger, M., and J. Burrows, Tropospheric sulfur dioxide observed by the ERS-2 GOME instrument, *Geophys. Res. Lett.*, *25*, 4177–4180, 1998.

Formenti, P., et al., Aerosol optical properties and large-scale transport of air masses: Observations at a coastal and a semiarid site in the eastern Mediterranean during summer 1998, *J. Geophys. Res.*, *106*, 9807–9826, 2001.

Formenti, P., et al., STAAARTE-MED 1998 summer airborne measurements over the Aegean Sea, 1, Aerosol particles and trace gases, *J. Geophys. Res.*, *107*, doi:10.1029/2001JD001337, in press, 2002.

Forster, C., et al., Transport of boreal forest fire emissions from Canada to Europe, *J. Geophys. Res.*, *106*, 22,887–22,906, 2001.

Halthore, R. N., Measurements and modeling of shortwave irradiance components in cloud-free atmospheres, in *Recent Research Developments in Geophysical Research*, vol. 2, edited by S. G. Pandalai, pp. 125–139, Res. Signpost, Trivandrum, India, 1999.

Hänel, G., The properties of atmospheric aerosol particles as functions of the relative humidity at thermodynamic equilibrium with the surrounding moist air, *Adv. Geophys.*, *19*, 73–188, 1976.

Hansen, J., and L. Travis, Light scattering in planetary atmospheres, *Space Sci. Rev.*, *16*, 527–610, 1974.

Harrison, L., and J. Michalsky, Objective algorithms for the retrieval of optical depths from ground-based measurements, *Appl. Opt.*, *33*, 5126–5132, 1994.

Hartley, W. S., P. V. Hobbs, J. L. Ross, P. B. Russell, and J. M. Livingston, Properties of aerosols aloft relevant to direct radiative forcing off the mid-Atlantic coast of the United States, *J. Geophys. Res.*, *105*, 9859–9885, 2000.

Hess, M., P. Koepke, and I. Schult, Optical properties of aerosols and clouds: The software package OPAC, *Bull. Am. Meteorol. Soc.*, *79*, 831–844, 1998.

Hobbs, P. V., J. S. Reid, J. A. Herring, J. D. Nance, R. E. Weiss, J. L. Ross, D. A. Hegg, R. D. Ottmar, and C. Liousse, Particle and trace-gas measurements in the smoke from prescribed burns of forest products in the Pacific Northwest, in *Biomass Burning and Global Change*, edited by J. S. Levine, pp. 697–715, MIT Press, Cambridge, Mass., 1996.

Horvath, H., Atmospheric light absorption: A review, *Atmos. Environ., Part A*, *27*, 293–317, 1993.

Intergovernmental Panel on Climate Change, *Climate Change 2001, The Scientific Basis: Contribution of Working Group I to the Third Assessment Report of the International Panel on Climate Change*, edited by J. T. Houghton et al., Cambridge Univ. Press, New York, 2001.

Iqbal, M., *An Introduction to Solar Radiation*, 390 pp., Academic, San Diego, Calif., 1983.

John, W., S. Hering, G. Reischl, G. Sasaki, and S. Goren, Characteristics of Nuclepore filters with large pore size, II, Filtration properties, *Atmos. Environ.*, *17*, 373–382, 1983.

Kato, S., et al., A comparison of the aerosol thickness derived from ground-based and airborne measurements, *J. Geophys. Res.*, *105*, 14,701–14,717, 2000.

Key, J., *Streamer User's Guide*, 96 pp., Coop. Inst. for Meteorol. Satell. Stud., Univ. of Wisconsin, Madison, Wis., 2001. (Also available at http://stratus.ssec.wisc.edu/streamer/streamer/html)

Kotchenruther, R. A., and P. V. Hobbs, Humidification factors of aerosols from biomass burning in Brazil, *J. Geophys. Res.*, *103*, 32,081–32,089, 1998.

Kotchenruther, R. A., P. V. Hobbs, and D. H. Hegg, Humidification factors for atmospheric aerosols off the mid-Atlantic coast of the United States, *J. Geophys. Res.*, *104*, 2239–2251, 1999.

Martins, J. V., P. Artaxo, C. Liousse, J. S. Reid, P. V. Hobbs, and Y. J. Kaufman, Effects of black carbon content, particle size, and mixing on light absorption by aerosols from biomass burning in Brazil, *J. Geophys. Res.*, *103*, 32,041–32,050, 1998.

Mayol-Bracero, O. L., P. Guyon, B. Graham, G. Roberts, M. O. Andreae, S. Decesari, M. C. Facchini, S. Fuzzi, and P. Artaxo, Water-soluble organic compounds present in biomass burning aerosols over Amazonia, 2, Apportionment of the chemical composition and importance of the polyacidic fraction, *J. Geophys. Res.*, *107*, doi:10.1029/2001JD000522, in press, 2002.

McClatchey, R. A., R. W. Fenn, J. E. A. Selby, F. E. Volz, and J. S. Garing, Optical properties of the atmosphere, *Tech. Rep. AFCRL-71-0279*, 411 pp., Air Force Cambridge Res. Lab, Bedford, Mass., 1971.

Mukai, H., and Y. Ambe, Characterization of a humic acid-like brown substance in airborne particulate matter and tentative identification of its origin, *Atmos. Environ.*, *20*, 813–819, 1986.

Quinn, P. K., D. J. Coffman, V. N. Kapustin, T. S. Bates, and D. S. Covert, Aerosol optical properties in the marine boundary layer during the First Aerosol Characterization Experiment (ACE1) and the underlying chemical and physical aerosol properties, *J. Geophys. Res.*, *103*, 16,547–16,563, 1998.

Redemann, J., R. P. Turco, K. N. Liou, P. V. Hobbs, W. S. Hartley, R. W. Bergstrom, E. V. Browell, and P. B. Russell, Case studies of the vertical structure of the direct shortwave aerosol radiative forcing during TARFOX, *J. Geophys. Res.*, *105*, 9971–9979, 2000.

Riley, J. P., and R. Chester, *Introduction to Marine Chemistry*, Academic, San Diego, Calif., 1971.

Russell, P. B., J. M. Livingston, P. Hignett, S. Kinne, J. Wong, A. Chien, R. Bergstrom, P. Durkee, and P. V. Hobbs, Aerosol-induced radiative flux changes off the United States mid-Atlantic coast: Comparison of values calculated from Sun photometer and in situ data with those measured by airborne pyranometer, *J. Geophys. Res.*, *104*, 2289–2307, 1999.

Satheesh, S. K., and V. Ramanathan, Large differences in tropical aerosol forcing at the top of the atmosphere and Earth's surface, *Nature*, *405*, 60–63, 2000.

Schmid, B., et al., Clear sky closure studies of lower tropospheric aerosol and water vapor during ACE-2 using airborne Sun photometer, airborne in-situ, space-borne, and ground-based measurements, *Tellus, Ser. B*, *52*, 568–593, 2000.

Sheridan, P. J., and J. A. Ogren, Observations of the vertical and regional variability of aerosol optical properties over central and eastern North America, *J. Geophys. Res.*, *104*, 16,793–16,805, 1999.

Thakaekara, M., Solar spectrum data, in *Handbook of Chemistry and Physics*, 72nd ed., edited by D. R. Lide, CRC Press, Boca Raton, Fla., 1992.

Trentmann, J., M. O. Andreae, H.-F. Graf, P. V. Hobbs, R. D. Ottmar, and T. Trautmann, Simulation of a biomass burning plume: Comparison of model results with observations, *J. Geophys. Res.*, *107*, doi:10.1029/2001JD000410, in press, 2002.

Tsay, S.-C., K. Stamnes, and K. Jayaweera, Radiative energy budget in the cloudy and hazy Arctic, *J. Atmos. Sci.*, *46*, 1002–1018, 1989.

Wendisch, M., et al., Aerosol-radiation interaction in the cloudless atmosphere during LACE 98, 1, Measured and calculated solar and spectral surface insolations, *J. Geophys. Res.*, *107*, doi:10.1029/2000JD000226, in press, 2002.

Wex, H., C. Neusüß, M. Wendisch, F. Stratmann, C. Koziar, A. Keil, A. Wiedensohler, and M. Ebert, Particle scattering, backscattering, and absorption coefficients: An in-situ closure and sensitivity study, *J. Geophys. Res.*, *107*, doi:10.1029/2000JD000234, in press, 2002.

Zerefos, C., K. Ganev, K. Kourtidis, M. Tzortziou, A. Vasaras, and E. Syrakov, On the origin of SO_2 above Northern Greece, *Geophys. Res. Lett.*, *27*, 365–368, 2000.

M. O. Andreae, O. Boucher, T. Reiner, and D. Sprung, Max Planck Institute for Chemistry, D-55028 Mainz, Germany.

P. Formenti, Centre of Geophysics of Évora, 7000-671 Évora, Portugal. (pfo@uevora.pt)

D. Kindred, Meteorological Research Flight, Met Office, GU146 TD Farnborough, UK.

M. Tzortziou, A. Vasaras, and C. Zerefos, Laboratory of Atmospheric Physics, Aristotle University, 540 06, Thessaloniki, Greece.

M. Wendisch and H. Wex, Institute for Tropospheric Research, 04303 Leipzig, Germany.